Check for updates

Harnessing a carbon-based material from food waste digestate for dye adsorption: the role of hydrogel beads in enhancing the material stability and regenerative capacity†

Salaheddine Farsad, [ID] *[a] Asma Amjlef,[a] Ayoub Chaoui,[a] Aboubakr Ben Hamou, [ID] [a] Chaima Hamma,[a] Mohamed Benafqir, [ID] [a] Amane Jada[bc] and Noureddine El Alem*[a]

This study focuses on both ecological and economic gains from food waste treatment. Accordingly, anaerobic digestion and adsorption have been combined to achieve these goals, resulting in synergistic effects that improve productivity. Firstly, a considerable amount of methane (energy source) was produced by the anaerobic digestion of food waste (FW) under mesophilic conditions (38 °C), resulting in a biologically activated digestate. Secondly, the residue of anaerobic digestion (digestate) was utilized as raw material to design two types of low-cost adsorbents for dye removal: a carbon-based material (CM-HNO$_3$) and an alginate encapsulated carbon-based material (CM-HNO$_3$@Alginate beads). We evaluated the adsorption capacity of the designed carbon materials to eliminate the target pollutant methylene blue (MB) from aqueous solutions. The results show that the CM-HNO$_3$ and CM-HNO$_3$@Alginate beads present maximum dye adsorption capacities of 303.03 mg g^{-1} and 212.77 mg g^{-1}, respectively. Further, the adsorption process was found to fit best to the Langmuir and pseudo-second-order kinetic models for both the adsorbents. In addition, the CM-HNO$_3$@Alginate beads exhibited good long-term stability, regenerative ability, and high mass recovery, indicating that this absorbent is suitable for frequent usage.

1. Introduction

Compared to the municipal waste, food waste (FW) constitutes over one-third of all urban waste resulting from anthropogenic activities and hence can be considered the most significant kind of solid waste across the world that needs to be suitably treated to achieve environmental sustainability.[1,2] Many approaches have been developed for food waste disposal (*e.g.*, incineration, landfilling, and composting).[3] Additionally, anaerobic digestion (AD) is one of the most economical and ecological processes employed for food waste bio-valorisation, which allows for the decomposition of complex organic matter in the waste through the intervention of micro-organisms in the absence of oxygen to produce bio-methane.[4] Bio-methane is regarded as a renewable energy source that does not lead to the exhaustion of fossil fuel supplies derived from petroleum and

charcoal briquettes, which cause climate change and global warming.[5,6] Nevertheless, the incomplete fermentation of food waste generates a massive quantity of food waste digestate (FWD): a by-product that should be properly managed and treated to ensure it does not cause environmental harm. Furthermore, previous studies have investigated the reuse of FWD as a biofertilizer or soil conditioner after proper treatment, since it contains a significant percentage of nutrients, especially nitrogen, phosphorus, and potassium.[7] However, there is a controversy surrounding this approach owing to the detrimental impacts of its other components, including heavy metals, photogenic bacteria, greenhouse gas (GHG) emissions, antibiotics, pesticides, and odour.[8]

Furthermore, value-added products, such as biochar-derived digestate, have been also developed as outstanding adsorbents and catalysts for pollutant removal from water.[9] Various kinds of solid digestate feedstocks may be used to prepare biochar materials, including municipal sludge,[10] rice straw,[11] and swine manure.[12] In addition, FWD is preferred for its lack of heavy metals and high nutrient content compared to other digestates.[13] Biochar is a black, low-cost, and porous carbonaceous material obtained from thermal decomposition (typically between 300 °C and 700 °C) of organic waste under an

[a] *Laboratory of Materials and Environment, Ibn Zohr University, Agadir, 80000, Morocco. E-mail: farsadsalaheddine@gmail.com, n.elalem@uiz.ac.ma*

[b] *Institute of Materials Science of Mulhouse (IS2M), Haute Alsace University, Mulhouse 68100, France*

[c] *Strasbourg University, Strasbourg 67081, France*

† Electronic supplementary information (ESI) available. See DOI: https://doi.org/10.1039/d3ma00505d

oxygen-free atmosphere.[14] Typically, the characteristics of biochar, such as pH, high surface content of oxygen-containing functional groups, electrical surface charge, and surface area, are largely dependent on the biomass feedstock and the inert/oxidizing conditions. In a study by Zhao et al.,[15] the pyrolysis performance of FW and FWD were compared in terms of their effects on biochar properties. These authors have shown that FWD pyrolysis promotes a higher yield of char with a high surface area, which has the potential to offer great adsorption performance and active sites for contaminant removal. Some recent papers have shown the feasibility of using FWD as feedstock for the modification of carbon based on pyrolysis processing methods. For instance, Liu et al.,[16] developed an FWD-based calcium-rich biochar to serve as an excellent arsenic(III) adsorbent. A maximum adsorption efficiency of 69.03 mg g^{-1} was obtained for this material by using the Langmuir isotherm adsorption model and an exothermic chemisorption process. Moreover, in another work, food waste digestate and 3 wt% sodium silicate binder were pyrolysed at 700 °C to prepare biochar, which was used as an adsorbent for heavy metal removal.[17] More than a six-fold increase was achieved compared with commercial activated carbon, and 355.3 mg g^{-1} of lead was removed, as determined by using the Langmuir isotherm model. However, biochar is typically not as effective at adsorption as activated carbon.[18,19]

Therefore, the purpose of this work is to prepare activated carbon from the digestate of food waste using a chemical activation procedure using HNO$_3$ to enhance the adsorption capacity. To our knowledge, the preparation of activated carbon from the digestate of food waste and the HNO$_3$ treatment of the carbon-based material adsorbent for enhanced methylene blue (MB) removal from water have not been reported.

Nevertheless, it is noteworthy that poor adsorbent recovery and mass loss after the decontamination of polluted water using powder materials are drawbacks that need to be overcome. Sodium alginate is a natural biodegradable polymer that is rich in oxygen-containing surface groups, non-toxic and biodegradable, and can be cross-linked with calcium cations to prepare hydrogel beads.[20–22] Hence, in order to resolve the problem of solid/liquid phase separation, several studies have investigated encapsulating alginate beads with carbonaceous materials to create a sustainable and stable spherical-shaped adsorbent for the removal of dyes,[23,24] pesticides,[25,26] heavy metals,[27] and drugs.[28]

This paper investigates the potential of anaerobic fermentation and adsorption to achieve zero waste and promote environmental protection by valorising food waste. Anaerobic digestion was employed to reduce pollution load and produce methane gas from food waste under mesophilic conditions (38 °C). However, disposal of the large amount of digestate produced during anaerobic digestion is difficult. To address this issue, two types of carbonaceous materials were developed from the digestate, both of which were effective adsorbents of methylene blue. Moreover, the physical and chemical characteristics of the synthesized carbonaceous materials and the effects of reaction parameters, including contact time, pH, initial dye concentration, thermodynamic study, regeneration, and adsorption mechanism, on their adsorption efficiency in batch mode have been discussed in detail.

In the context of circular bioeconomy, this study makes a significant contribution toward efficiently converting food waste digestate (FWD) into valuable carbon materials, thus reducing waste and promoting resource efficiency. Additionally, it aligns with a range of Sustainable Development Goals (SDGs), including SDG 6 (Clean Water and Sanitation), SDG 7 (Affordable and Clean Energy), SDG 12 (Responsible Consumption and Production), and SDG 13 (Climate Action). By addressing these global sustainability objectives, this research offers a significant solution toward tackling environmental challenges and advancing sustainable practices.

2. Materials and methods

2.1. Food waste sample

A mixture of food waste consisting mainly of vegetable and fruit peelings from the kitchen was used as the substrate. The composition of the substrate was as follows: 22% potato, 20% apple, 18% tomato, 10% pumpkin, 9% banana, and the remaining 21% consisted of a combination of orange, lettuce, cauliflower, carrot, and cucumber peels. The substrate was ground and homogenized using a food blender to obtain a finer raw material. The pH of the substrate was 4.14, while its total solid (TS) and volatile solid (VS) concentrations were 88.6 g L^{-1} and 79.6 g L^{-1}, respectively. The food waste was processed and homogenized before being stored at −20 °C until further use. The details of the experimental design and characterization of the anaerobic fermentation of the food waste are provided in ESI.†

2.2. Carbonaceous material preparation

From the food waste digestate, two forms of carbonaceous materials (CM-HNO$_3$ and CM-HNO$_3$@Alginate beads) were developed in order to study their dye adsorption performance.

The experimental protocol used for the preparation of the oxidized carbonaceous materials (CM-HNO$_3$) can be divided into several steps. Initially, the residue (bio-digestate) produced from the anaerobic fermentation of household organic waste was dried at 40 °C for 24 hours and then at 200 °C for 4 hours in the air. The final product was ground into a fine powder in a ceramic mortar, screened with a sieve and then placed in a closed alumina crucible that was hermetically sealed with several layers of aluminium foil and placed in a furnace at 500 °C for 4 h. Then, using nitric acid HNO$_3$ (4N), the obtained product was activated at 70 °C for 12 h. The filtrate was washed with distilled water and ethanol and then dried for 24 hours at 100 °C.

The production of CM-HNO$_3$@Alginate beads for this study involved several steps. First, 1 g of alginate powder and 1 g of CM-HNO$_3$ were dissolved in 100 mL of distilled water, and the resulting mixture was stirred for 6 hours. After agitation, the mixture was sonicated for 20 minutes to enhance the

dispersion and homogenization of CM-HNO$_3$ and alginate. Meanwhile, a CaCl$_2$ (0.1 M) solution was prepared in a crystallizer under low-speed stirring (30 rpm), and the preparation of the CM-HNO$_3$@Alginate beads was achieved by mixing the two solutions.

2.3. Characterization of carbonaceous materials

As a part of our work, the crystalline structures of the carbonaceous materials and oxidized materials were determined by X-ray diffraction (XRD) (Bruker D8 Advance Twin) in the angular 2θ range of 5° to 60° using Cu Kα radiation λ = 0.15418 nm (40 kV and 25 mA). The functional groups of methylene blue (MB) and CM-HNO$_3$ were determined using a SHIMADZU IRAffinity-1S FTIR spectrometer over a wavenumber range of 400–4000 cm^{-1}. To prepare the FTIR test samples, 1% of each adsorbent was ground finely and pressed with 99% KBr. The analysis of the thin pellets was conducted by scanning at a resolution of 4 cm^{-1}. In order to examine the microstructure and morphology of the CM-HNO$_3$ and CM-HNO$_3$@Alginate bead surfaces, scanning electron microscopy (SEM) analysis was performed using a JEOL JSM IT-100 coupled with an energy-dispersive X-ray spectrometer, which allowed determination of the local elemental compositions in different zones. After the powders were glued to double-sided carbon tape, gold was deposited using the cathode sputtering method with a metallizer.

2.4. Batch-mode dye adsorption studies

Methylene blue (MB), belongs to the large family of cationic dyes widely used in textile production. A batch system was used to test the removal of MB dye molecules from an aqueous solution using CM-HNO$_3$ and the CM-HNO$_3$@Alginate beads particles. Thus, MB in solution (20 mg L^{-1}) was adsorbed onto a known dose of CM-HNO$_3$ and CM-HNO$_3$@Alginate beads (0.8 g L^{-1}). The effects of some parameters were investigated by varying the pH of the dye solution in the range of 2–12 using a few drops of HCl and NaOH (0.1 M) solutions, and the contact time was varied between 0 and 270 min. At the end of each adsorption experiment, the non-adsorbed MB molecules were separated from the solution by using a filtration method, and the concentration of remaining MB in the solution was analyzed by a UV-visible spectrophotometer (6705 UV-visible JENWAY) at λ = 664 nm. The formulas utilized in the kinetic and equilibrium studies of MB adsorption on CM-HNO$_3$ and CM-HNO$_3$@Alginate beads are provided in Table S3 (ESI†).

2.5. Regeneration and reusability

Regenerating used adsorbents in practical applications ensures the economic feasibility of the adsorption process, and it gives a clear idea about the stability and reusability of the adsorbents. To generate an adsorbent fully loaded with MB, 200 mL of an MB solution with a suspension containing 160 mg CM-HNO$_3$ or CM-HNO$_3$@Alginate beads was shaken for 120 min and 240 min, respectively, at room temperature. The separation of the CM-HNO$_3$ adsorbent from the MB/adsorbent mixture was achieved through vacuum filtration, followed by rinsing the MB-covered adsorbent with distilled water. The resulting solid

phase was further mixed and shaken for 6 h with 100 mL 0.1 mol L^{-1} NaOH solution at ambient temperature; afterward, the obtained solid fraction was dispersed in a 0.1 mol L^{-1} aqueous HCl solution for 2 hours, washed with distilled water, and finally dried. To recover the CM-HNO$_3$@Alginate beads, the adsorbent containing the MB molecules was first washed thoroughly in 100 mL 0.1 mol L^{-1} HCl solution. Thereafter, the resulting solid fraction consisting of bare CM-HNO$_3$@Alginate beads was recovered by magnetic stirring for 2 hours. For the next MB adsorption cycle, both bare CM-HNO$_3$ and CM-HNO$_3$@Alginate adsorbents were again mixed and agitated with fresh MB solutions. The regeneration efficiency was assessed over 5 cycles by measuring the amount of MB adsorbed after each cycle and determining the remaining MB concentration.

3. Results and discussion

3.1. Anaerobic digestion process optimization and methane production

It is essential to recognize that the anaerobic digestion process in batch digesters is subject to a multitude of variables. In order to evaluate the exhaustive impact of these parameters on the production of methane, in this study, three specific factors were systematically investigated through a series of four experimental trials, as detailed in Table S2 (ESI†). Notably, among the different conditions tested, the highest methane yield was obtained by using the substrate stored previously for two days at a pH of 7.5 and 25% inoculum. A closer look at the methane production data revealed several remarkable findings. Firstly, maintaining a pH close to neutral (pH = 7.5) resulted in maximum microbial growth compared with pH values closer to the intrinsic pH of the substrate (acidic). This observation highlights the critical influence of pH regulation on the anaerobic digestion process. Secondly, inoculum percentage emerged as a key determinant of the methane production process. Specifically, at an inoculum concentration of 25%, the study revealed highly promising and substantial methane production. This highlights the importance of optimizing the inoculum level to improve the efficiency of anaerobic digestion processes. Finally, the duration of substrate storage before the anaerobic digestion process was identified as an important factor impacting methane production. The results demonstrated that longer storage periods significantly improved methane yields, highlighting the potential benefits of using storage as a pretreatment method to improve the anaerobic digestion performance. These results collectively provide valuable insights into the optimization of the anaerobic digestion process parameters and the interaction between various parameters and their crucial roles in methane production.

Similar research conducted by B. Deepanraj *et al.*, examined the positive effect of neutral pH (pH = 7) on the anaerobic fermentation of food waste studied in the pH 5–9 range in 2L batch bioreactor experiments with 30 days of hydraulic retention at mesophilic temperatures.[29] Another study done by Lü

et al., found that storage can be used as a pre-treatment to improve the performance of anaerobic fermentation of food waste; they studied food wastes without and with substrate storage for 0, 1, 2, 3, 4, 5, 7, and 12 days. The results showed that stored food waste offered good methane yields compared to non-stored samples.[30] Regarding inoculum percentage, S. Farsad *et al.* studied its effect on the mesophilic anaerobic digestion of landfill leachate and found that compared with 50%, at 25% inoculum, a higher methane yield was obtained.[31]

3.2. Carbonaceous material characterization

3.2.1. XRD and FTIR analyses. The X-ray diffraction results for CM and CM-HNO$_3$ are shown in Fig. 1(a). The diffraction peaks observed at various angles $2\theta = 74.09$, 68.17, 58.64, 50.59, 45.29, 40.64, 38.09, 32.38, and 28.56 are due to the remaining mineral content in food waste (mainly KCl, and Na$_2$CO$_3$). After the chemical activation of CM, the mineral components were eliminated, and graphitic carbon was formed, as evidenced by the disappearance of the KCl, and Na$_2$CO$_3$ peaks (CM-HNO$_3$(a) in Fig. 1(a)). The peak occurring at $2\theta = 26.66$ is attributed to

graphite structure, indicating the crystallized part of CM-HNO$_3$. The reticular distance of the 002 plane, as calculated from XRD, was of the order of 3.34 Å, which is close to the theoretical range for graphite (3.354–3.44 Å).

Fig. 1(b) shows the FTIR spectra of methylene blue (MB) and CM-HNO$_3$ before and after MB adsorption. The functional groups identified in pure MB include bonded –OH groups (3442 cm^{-1}), C=O and C=C aromatic vibrations (1602 cm^{-1}),[32] CH$_2$ deformation vibration (1489 cm^{-1}), C–N bonds in the heterocycle (1392 cm^{-1}), C–N bonds connected with the benzene ring (1359 cm^{-1}), C–S bonds (1178 cm^{-1}), and the wagging vibration of C–H in the aromatic ring (887 cm^{-1}).[33]

The main functional groups of CM-HNO$_3$ are represented by peaks at 3205 cm^{-1} (bonded –OH groups), 1699 cm^{-1} (organic residues and carboxyl functional groups),[34] 1581 cm^{-1} (the stretch vibration of C=C),[35] 1386 cm^{-1} (C–O stretching vibration),[32] and 1082 cm^{-1} (C–O stretching),[35] and the peaks between 520 and 906 cm^{-1} confirm the out-of-plane bending vibration of the –C–H bond on the benzene ring.[36]

After the adsorption of MB onto CM-HNO$_3$, certain peaks either shifted or appeared. The peaks at 3205 cm^{-1}, 1699 cm^{-1}, 1581 cm^{-1}, and 1386 cm^{-1} shifted respectively to 3375 cm^{-1}, 1703 cm^{-1}, 1593 cm^{-1}, and 1396 cm^{-1}, indicating that the carboxyl functional groups, namely C=C, –OH and C–O, were involved in the adsorption process, and the appearance of new peaks at 1489 cm^{-1} and 1178 cm^{-1} can be attributed to the presence of MB molecules on the surface of the material, which proves that MB was successfully adsorbed by the material.

3.2.2. MEB analysis. The surface morphologies of CM-HNO$_3$ and the CM-HNO$_3$@Alginate beads before and after MB adsorption were examined by SEM analysis.

The CM-HNO$_3$ sample exhibited distinctive cavities and pores (Fig. 2(a)), which can be attributed to the strong oxidizing ability of nitric acid. The resulting pores provide favourable adsorption sites for MB. This observation is corroborated by the data presented in Fig. 2(c), which demonstrates that MB filled all the pores and cavities on the surface of CM-HNO$_3$. Fig. 2(b), (d), (e), (f) show the more comprehensive energy-dispersive X-ray elemental mappings (EDX) that verify the chemical composition data at specific locations on CM-HNO$_3$ before and after MB adsorption. Apparently, Fig. 2(b) and (e) reveal the presence of carbon (71.82%) and oxygen (28.18%), confirming the graphitic structure of the synthesized CM-HNO$_3$. After the adsorption of MB, the EDX spectrum of CM-HNO$_3$ (Fig. 2(d) and (f)) revealed the presence of additional elements, namely nitrogen (1.84%) and sulfur (0.42%), confirming that the MB molecules were successfully adsorbed on the surface of CM-HNO$_3$.

Additionally, the structure of the prepared CM-HNO$_3$@Alginate beads was investigated using SEM (Fig. 3(a), (b) and (e)). The results show that the oxidized carbonaceous materials were trapped inside a membrane-like layer, confirming their combination by the complexation of the –COOH groups of alginate and the calcium ions Ca^{2+}. This layer formed a shell around the hydrogel beads, giving them a spherical shape (Fig. 3(a)). Similarly, when MB was adsorbed into CM-HNO$_3$@Alginate (Fig. 3(a), (b), (e)), the SEM and mapping
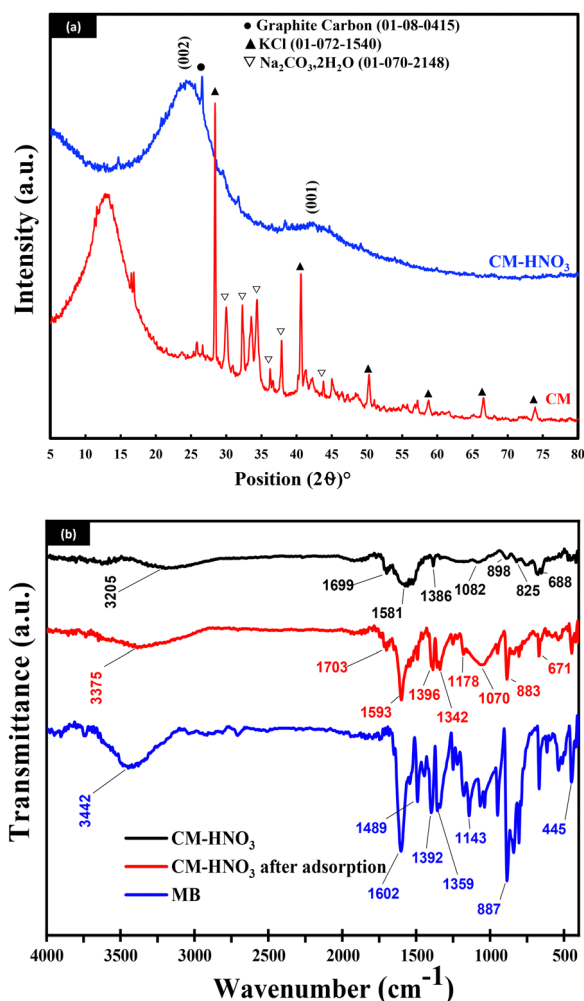

Fig. 1 (a) The XRD patterns of CM and CM-HNO$_3$; (b) the FTIR spectra of CM-HNO$_3$, CM-HNO$_3$ after adsorption, and MB.
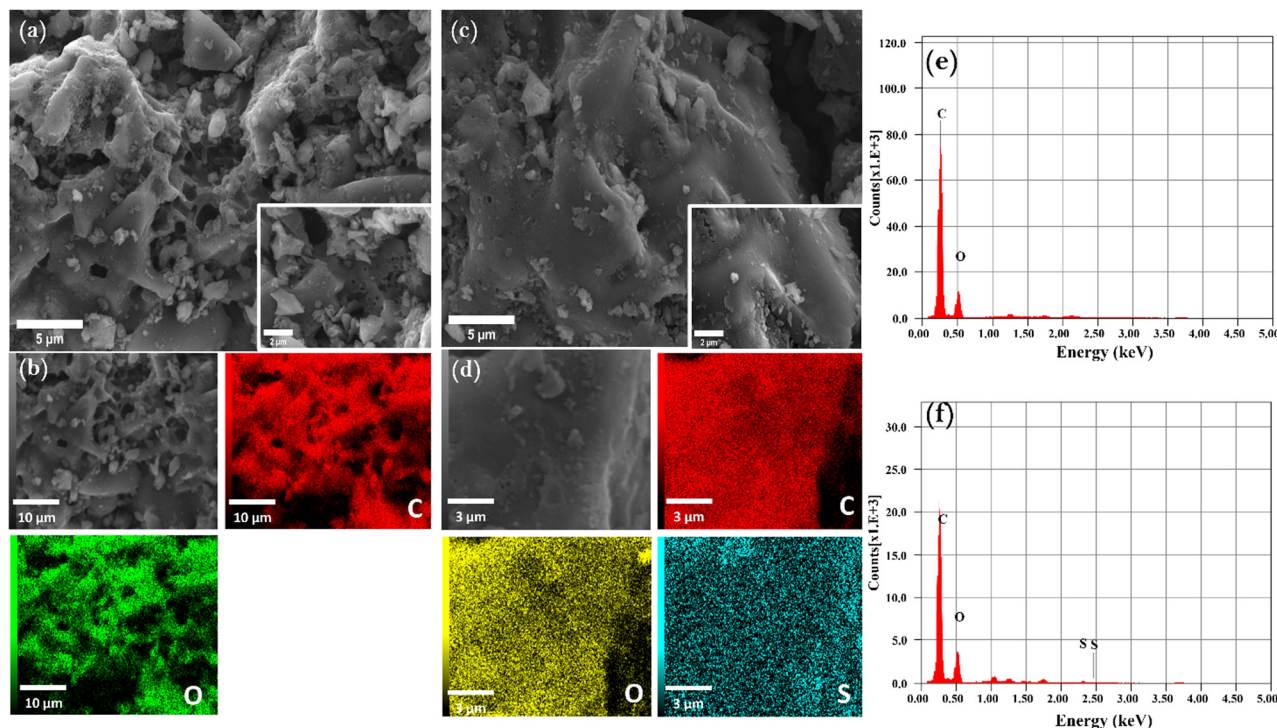
Fig. 2 The SEM and elemental mapping analyses of CM-HNO$_3$ (a), (b), (e) before and (c), (d), (f) after MB adsorption.

analyses indicated the presence of sulfur (3.4%) alongside carbon (63.35%), oxygen (32.91%), and calcium (0.34%), confirming the adsorption of MB molecules on the surface of the CM-HNO$_3$@Alginate beads.

3.3. MB adsorption

3.3.1. Effect of solution pH. The influence of pH on the adsorption process is important as it significantly affects the surface charge characteristics of the adsorbent material and governs the interfacial dynamics between the adsorbent and the adsorbate species. As such, considering the effect of pH is of utmost importance in comprehending and optimizing the adsorption process.[37] The effect of pH on MB adsorption onto CM-HNO$_3$ and CM-HNO$_3$@Alginate was studied over a wide pH range of 2–12. The results are presented in Fig. 4(a). At pH values between 2 and 6, the removal efficiency of MB was constant and less than 50% for both adsorbents, which may be due to the protonation of the surface sites of the adsorbents. However, when the pH was higher than 6, the MB removal efficiency gradually increased and reached the maximum at pH 12. This can be explained by the deprotonation of the active sites of the adsorbents, and negatively charged sites promoting electrostatic attraction with the MB molecules. The maximum MB removal efficiency was found to be 88% and 67% for CMHNO$_3$ and CM-HNO$_3$@Alginate, respectively. Therefore, pH 12 was chosen as the optimal pH for subsequent experiments.

3.3.2. Effect of contact time and kinetic studies. To elucidate the mechanism of adsorption of MB on CM-HNO$_3$ and CM-HNO$_3$@Alginate,[38] the effect of contact time and

adsorption kinetics were studied. The experiments were performed at the following conditions: contact time = 0–270 min, adsorbent dosage = 0.8 g L^{-1}, C_0 (MB) = 20 mg L^{-1}, pH = 12, and T = 25 °C.

From Fig. 4(b), it can be seen that the adsorption capacity of CM-HNO$_3$ and CM-HNO$_3$@Alginate increased rapidly during the first 60 min due to the availability of active sites on the surface of the adsorbents.[39] After 60 min, a slow increase in adsorption capacity was observed due to the decrease in the number of active sites on the adsorbent surface. Moreover, there was no significant change in the adsorption capacity after 120 min and 240 min for CM-HNO$_3$ and CM-HNO$_3$@Alginate, respectively. These findings indicate that the adsorbate–adsorbent contact times 120 min and 240 min are the equilibrium times for CM-HNO$_3$ and the CM-HNO$_3$@Alginate, respectively. The adsorption kinetics results were compared to the pseudo-first-order and pseudo-second-order theoretical models Fig. 4(c), (d). From Table 1, it can be seen that the correlation coefficient values for the pseudo-second-order kinetic model (R^2 > 0.99) were higher compared with those for the pseudo-first-order model for both adsorbents (CM-HNO$_3$ and CM-HNO$_3$@Alginate). On the other hand, the values of Q_{cal} calculated from the pseudo-second-order model were similar to the experimental values. Therefore, the pseudo-second-order model better describes the adsorption kinetics of MB onto CM-HNO$_3$ and CM-HNO$_3$@Alginate.[40]

3.3.3. Effect of initial concentration and adsorption isotherms. In order to gain insights into the adsorption mechanism of MB onto CM-HNO$_3$ and CM-HNO$_3$@Alginate, the adsorption isotherms were studied. The experiments were
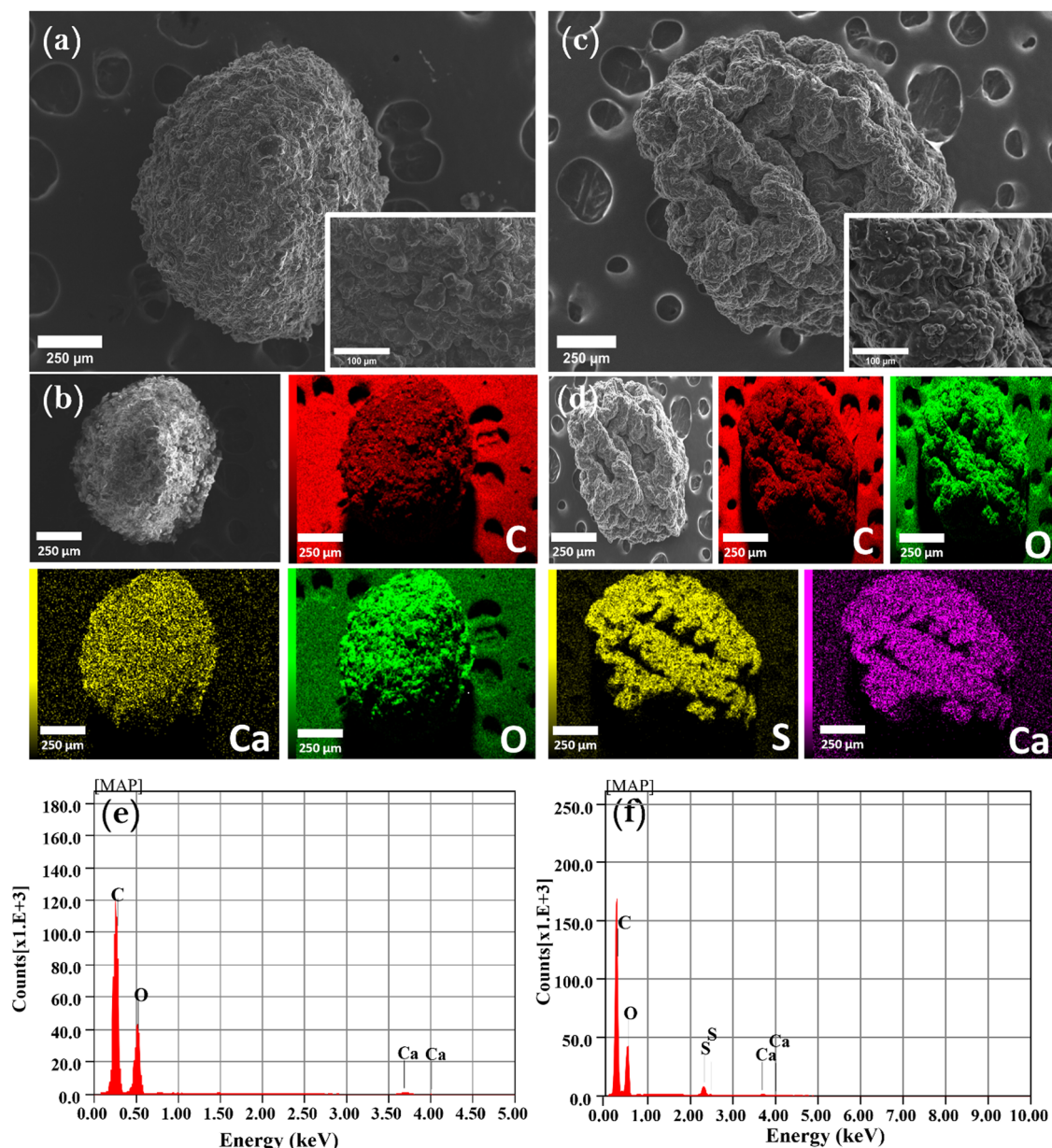
Fig. 3 The SEM and mapping analyses of CM-HNO$_3$@Alginate beads (a), (b), (e) before and (c), (d), (f) after MB adsorption.

performed at the following conditions: C_0 (MB) = 0–600 mg L^{-1}, adsorbent dosage = 0.8 g L^{-1}, pH = 12, T = 25 °C, and the contact time was 120 min and 240 min for CM-HNO$_3$ and CM-HNO$_3$@Alginate, respectively.

The adsorption isotherms were investigated using the linear regression analysis of Langmuir and Freundlich. The results are demonstrated in Fig. 5 and Table 2. The values of the coefficients of correlation R^2 found by Langmuir were 0.9731 and 0.9178 for CM-HNO$_3$ and CM-HNO$_3$@Alginate, respectively. However, the values of correlation coefficients R^2 found by Freundlich were 0.8962 and 0.8169 for CM-HNO$_3$ and CM-HNO$_3$@Alginate, respectively. The Langmuir model exhibited the highest correlation coefficient, indicating that it most appropriately describes the adsorption behaviour of MB onto

CM-HNO$_3$ and CM-HNO$_3$@Alginate. Therefore, MB dye adsorption onto the CM-HNO$_3$ and CM-HNO$_3$@Alginate adsorbents occurs in monolayers on homogeneous surfaces.[41] The Q_{max} values obtained by the Langmuir model were 303.03 mg g^{-1} and 212.77 mg g^{-1} for CM-HNO$_3$ and CM-HNO$_3$@Alginate, respectively. The values of R_L were 0.0308 (CM-HNO$_3$) and 0.0147 (CM-HNO$_3$@Alginate). These values are between 0 and 1, confirming that the adsorption of MB onto CM-HNO$_3$ and CM-HNO$_3$@Alginate is favourable.[42]

3.3.4. Thermodynamic studies. For a better comprehension of the thermodynamic behavior of the adsorption of MB onto CM-HNO$_3$ and CM-HNO$_3$@Alginate, the thermodynamic parameters (Gibbs free energy ($\Delta G°$), enthalpy ($\Delta H°$), and entropy ($\Delta S°$)) were determined according to the van't Hoff
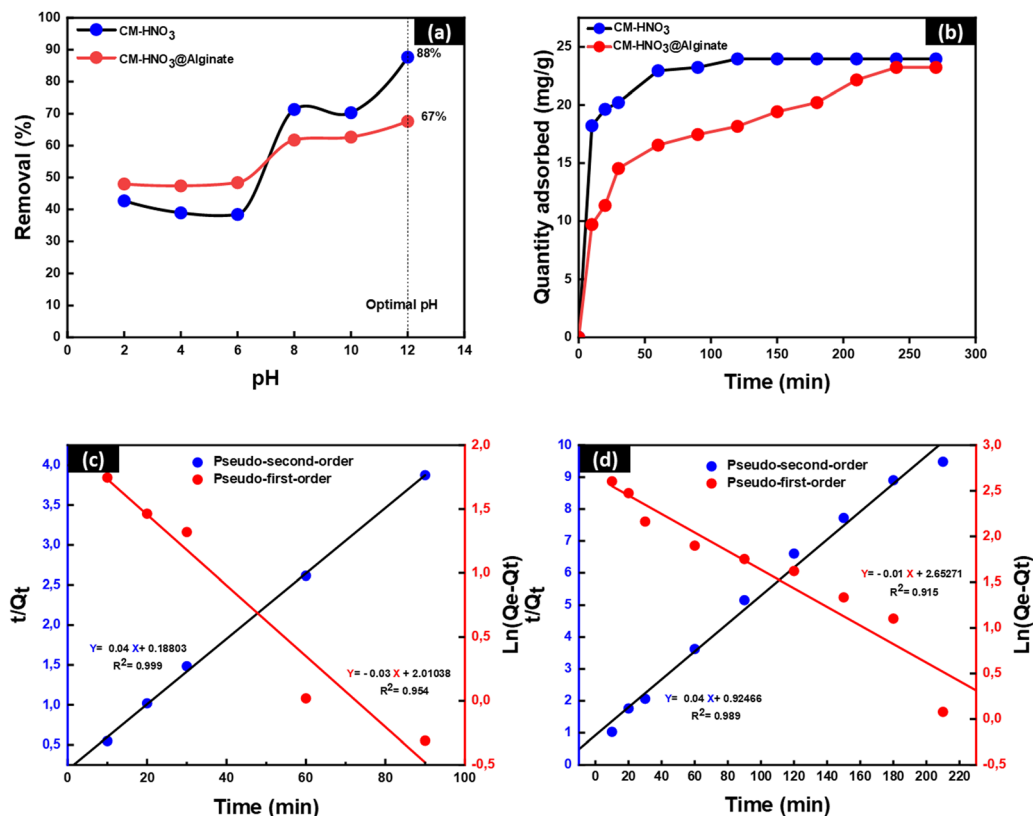
Fig. 4 The effect of (a) pH and (b) contact time on the adsorption of MB. Adsorption kinetics of MB on (c) CM-HNO$_3$ and (d) CM-HNO$_3$@Alginate.

Table 1 Kinetics parameters for the adsorption of MB onto CM-HNO$_3$ and CM-HNO$_3$@Alginate

		CM-HNO$_3$	CM-HNO$_3$@Alginate
Pseudo-first-order model	$Q_{e,exp}$ (mg g^{-1})	23.226	23.122
	$Q_{e,cal}$ (mg g^{-1})	7.463	14.241
	K_1 (min^{-1})	0.028	0.011
	R^2	0.9541	0.909
Pseudo-second-order model	$Q_{e,cal}$ (mg g^{-1})	24.814	24.096
	K_2 (min^{-1})	0.008	0.002
	R^2	0.9993	0.9854

equation by plotting ln(K_d) as a function of $1/T$ (Fig. 6(a) and (b)).[43] The thermodynamic coefficient values are presented in Table 3.

The negative ΔG° values indicate that MB adsorption onto CM-HNO$_3$ and CM-HNO$_3$@Alginate was spontaneous and more favoured with a temperature increase.[44] Further, the positive ΔH° values reveal that MB adsorption onto CM-HNO$_3$ and CM-HNO$_3$@Alginate are endothermic processes.[45] Finally, the positive ΔS° values suggest an increase in randomness at the interface (adsorbent–adsorbate) during the adsorption process.[46]

3.4. Reusability study

Besides their eco-friendliness and efficiency in removing organic pollutants from wastewater, the prepared CM-HNO$_3$ adsorbents must also be reused several times to investigate their performance for the removal of organic contaminants.

The reusability study was conducted in order to demonstrate the excellent adsorption properties of the adsorbents, as well as their ability to be recycled and reused. A total of five successive cycles of MB adsorption and desorption were conducted to remove the MB dye. Great sorption efficiency was recorded while using 0.1 M HCl as the regenerator. After five successive cycles of adsorption and desorption, the MB removal efficiency of CM-HNO$_3$ decreased gradually from 97% to 77%. In contrast, CM-HNO$_3$@Alginate revealed excellent recyclability with MB removal efficiency greater than 91%. These results indicate that the overall regeneration capacity of CM-HNO$_3$@Alginate is clearly higher than that of CM-HNO$_3$, as shown in Fig. 6(c).

3.5. Comparative assessment

The adsorption capacity of the prepared materials was compared with a range of adsorbents documented in the literature, and the results of this evaluation are presented in Table 4.
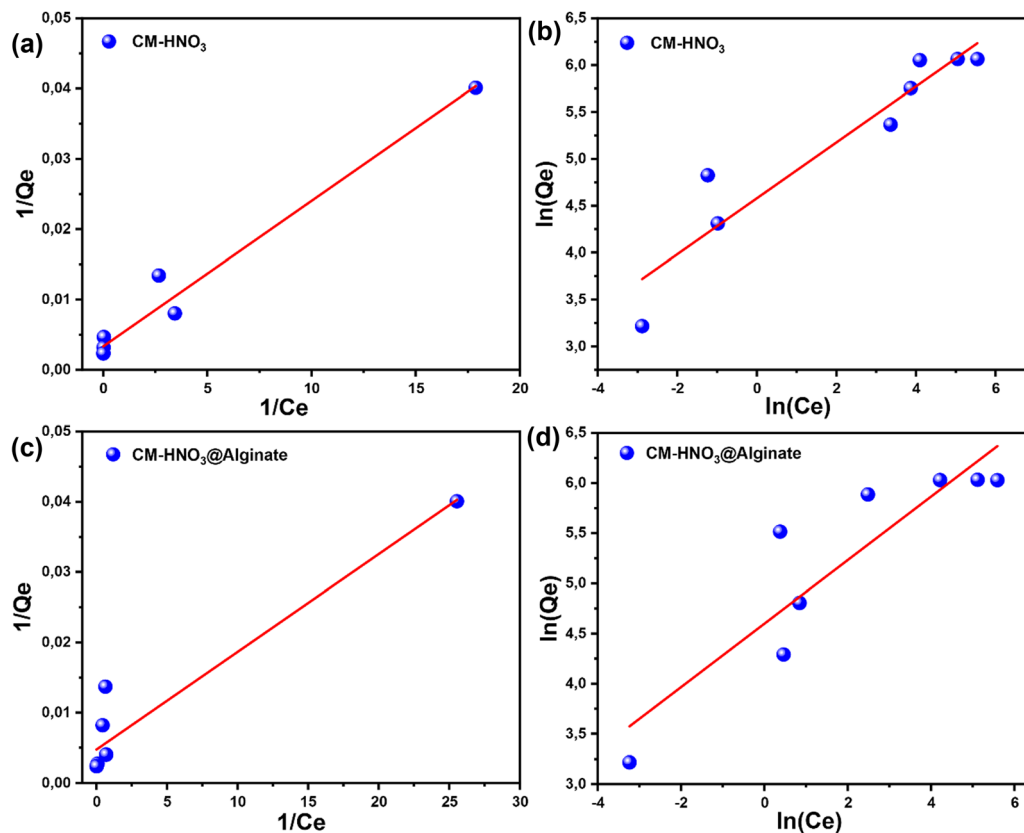
Fig. 5 The adsorption isotherms of MB on (a), (b) CM-HNO$_3$ and (c), (d) CM-HNO$_3$@Alginate.

Table 2 The Langmuir and Freundlich isotherm parameters for MB adsorption

	Langmuir				Freundlich		
	Q_{max} (mg. g^{-1})	K_L (L mg^{-1})	R^2	R_L	K_F (mg g^{-1}) (L mg^{-1})$^{1/n}$	n	R^2
CM-HNO$_3$	303.03	1.57	0.9731	0.0308	97.46	3.35	0.8962
CM-HNO$_3$@Alginate	212.77	3.35	0.9178	0.0147	99.37	3.16	0.8169

Notably, the prepared materials CM-HNO$_3$ and CM-HNO$_3$@Alginate exhibited outstanding adsorption performance in the removal of methylene blue (MB). This superior performance positions these materials among the most efficient adsorbents in the literature for the elimination of MB. The exceptional adsorption capacity demonstrated by these materials derived from food waste digestate suggests their potential as highly promising and competitive alternatives for effective MB removal from aqueous solutions.

3.6. The adsorption mechanism

The adsorption mechanism of methylene blue (MB) onto CM-HNO$_3$ is a multifaceted process characterized by simultaneous interactions. As depicted in Fig. 7, we propose a model to illustrate this process. The FTIR data of CM-HNO$_3$ before and after MB adsorption reveal slight changes in peak intensities along with the displacement of certain peaks. These shifts predominantly involve functional groups, such as carboxyl (–COOH), C=C, –OH, and C–O groups. Consequently, the primary mechanisms governing this adsorption process encompass hydrogen bonding interactions, π–π interactions, and electrostatic interactions.

Furthermore, the adsorption mechanism is notably influenced by pH. In particular, our findings suggest a significant role of electrostatic interactions in the adsorption process. Specifically, electrostatic interactions are presumed to arise from the attraction between the negative charge of the carboxylic anion in CM-HNO$_3$ and the positive charge on MB.[52] Additionally, hydrogen bonding interactions may form between the hydrogen atoms of CM-HNO$_3$ and the nitrogen atoms of MB.[53] Moreover, π–π interactions are likely to occur between the benzene ring structures in the MB molecules and the aromatic components of CM-HNO$_3$.[54]

Until recently, there have been limited reports concerning the mechanism of methylene blue adsorption onto biochar or activated carbon derived from food waste digestate. Biochar
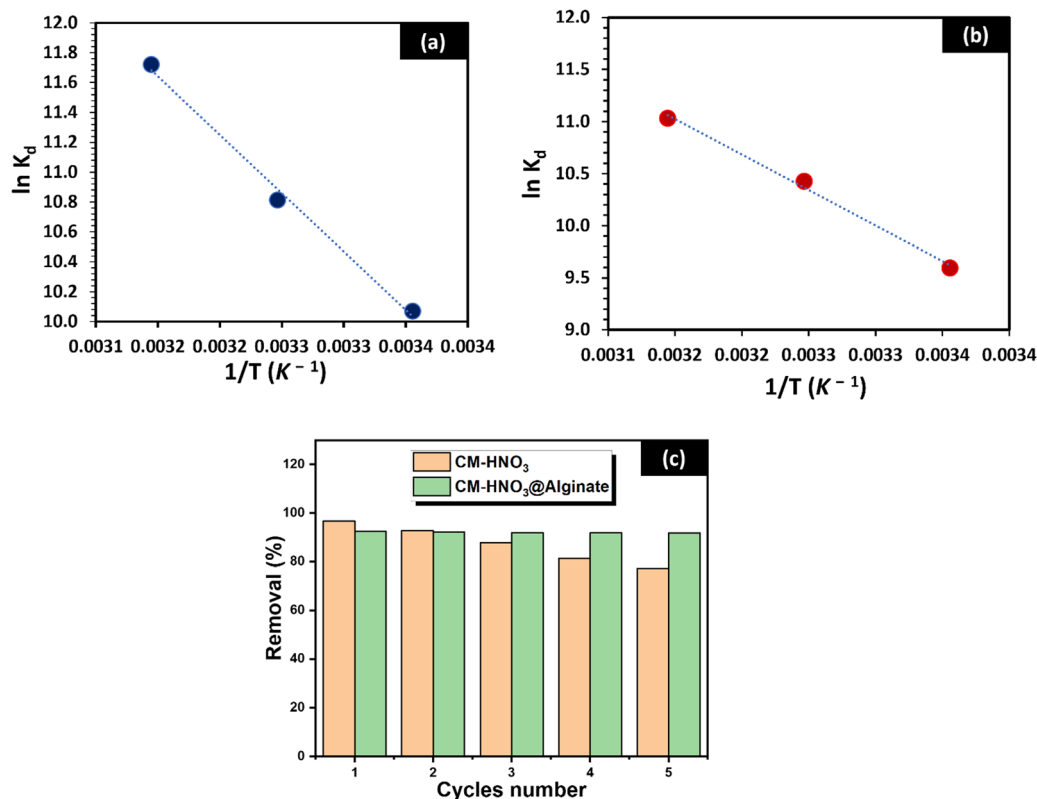
Fig. 6 The van't Hoff plot for MB adsorption onto (a) CM-HNO$_3$ and (b) CM-HNO$_3$@Alginate; (c) the reusability study of CM-HNO$_3$ and CM-HNO$_3$@Alginate.

Table 3 The thermodynamic parameters of CM-HNO$_3$ and CM-HNO$_3$@Alginate for MB removal

	ΔG° (kJ mol^{-1})			ΔH° (kJ mol^{-1})	ΔS° (J mol^{-1} K^{-1})
	298 K	308 K	318 K		
CM-HNO$_3$	−25.04	−27.47	−29.91	47.51	243.47
CM-HNO$_3$@Alginate	−23.84	−26.54	−29.24	56.70	270.27

Table 4 Comparison of the adsorption capacity of CM-HNO$_3$ and CM-HNO$_3$@Alginate with that of other reported adsorbents

Nature of adsorbent	Contaminants	Adsorption capacity	Ref.
Biochar prepared from the digestate of rice straw	Methylene blue (MB) in an aqueous solution	18.9 mg g^{-1}	47
Activated carbon prepared from the digestate of agri-food organic waste	Methylene blue (MB) in an aqueous solution	285.71 mg g^{-1}	35
Biochar from lychee seed	Methylene blue (MB) in an aqueous solution	124.5 mg g^{-1}	48
Hydrochar derived from coconut shell waste	Methylene blue (MB) in an aqueous solution	200.01 mg g^{-1}	49
Biochar from sewage sludge	Methylene blue (MB) in an aqueous solution	29.85 mg g^{-1}	50
Activated carbon prepared from the digestate of corn straw	Methylene blue (MB) in an aqueous solution	179.1 mg g^{-1}	51
CM-HNO$_3$ and CM-HNO$_3$@Alginate	Methylene blue (MB) in an aqueous solution	303.03 mg g^{-1} and 212.77 mg g^{-1}	This study

derived from food waste digestate exhibits alkaline characteristics and contains both oxygen-based functional groups on its surface, as well as inorganic mineral constituents.[55] The interaction mechanisms reported previously between other digestate absorbents and methylene blue involve the formation of electrostatic bonds and various types of bonds, such as π–π interactions, n–π interactions, and hydrogen bonding, through the oxygen-containing functional groups present on the surface of the digestate.[47,56]
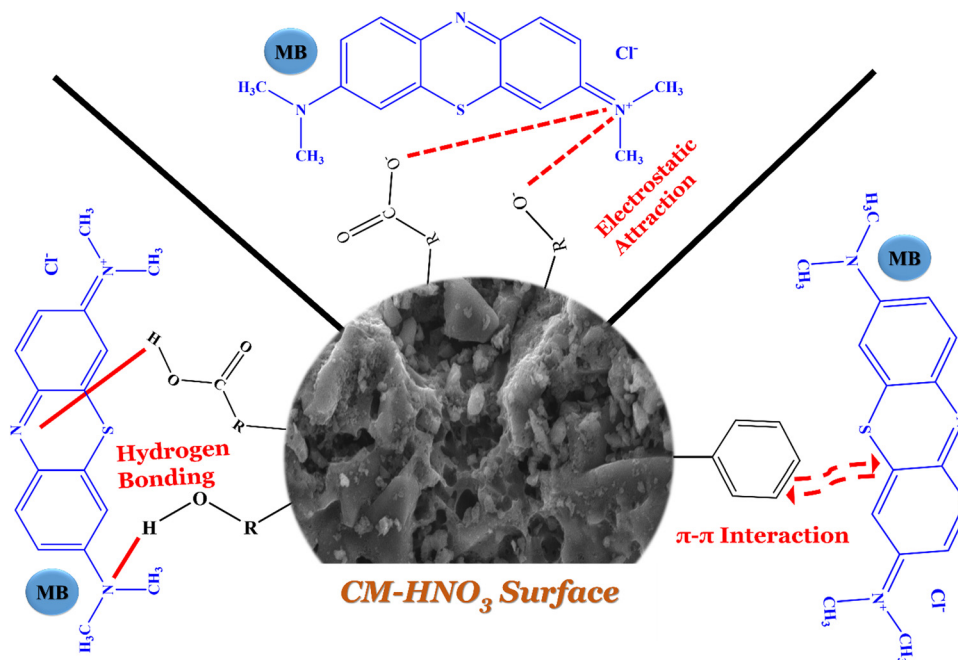
Fig. 7 The adsorption mechanism of the MB dye onto CM-HNO$_3$.

4. Conclusion

This work deals with the valorisation of food waste in order to achieve zero waste and promote environmental protection by using both anaerobic digestion and adsorption processes. The first part was focused on pollution load reduction and methane gas production from food waste under mesophilic conditions (38 °C). In the second part, the CM-HNO$_3$ and CM-HNO$_3$@Alginate adsorbents were prepared from the digestate. Both carbon-based adsorbents show good dye removal efficiencies, and various methods, such as XRD and FTIR, confirm their demineralization and formation of graphitic carbon structures after their chemical activation. Further, the experimental results show that the adsorption process depends on solution pH, and the optimum pH for dye removal is around 12. In addition, the kinetic study indicates a fast adsorption process for CM-HNO$_3$, while it takes a little longer for CM-HNO$_3$@Alginate, and their adsorption mechanism can be described by pseudo-second-order kinetics. Moreover, the study suggests that the CM-HNO$_3$@Alginate adsorbent has better stability, high mass recovery, and good reusability than CM-HNO$_3$ after five cycles of dye adsorption and desorption. Therefore, CM-HNO$_3$@Alginate can be a promising absorbent for frequent pollutant removal applications. Overall, this work is an important step towards the valorisation of food waste and promoting sustainable waste management practices.

Conflicts of interest

The authors have no conflicts of interest to declare.

Acknowledgements

References

1 M. Xu, M. Yang, H. Sun, J. Meng, Y. Li, M. Gao, Q. Wang and C. Wu, Role of multistage inoculation on the co-composting of food waste and biogas residue, *Bioresour. Technol.*, 2022, **361**, 127681, DOI: **10.1016/j.biortech.2022.127681**.

2 M. Kumar, S. Dutta, S. You, G. Luo, S. Zhang, P. L. Show, A. D. Sawarkar, L. Singh and D. C. W. Tsang, A critical review on biochar for enhancing biogas production from anaerobic digestion of food waste and sludge, *J. Cleaner Prod.*, 2021, **305**, 127143, DOI: **10.1016/j.jclepro.2021.127143**.

3 C. Zhang, H. Su, J. Baeyens and T. Tan, Reviewing the anaerobic digestion of food waste for biogas production, *Renewable Sustainable Energy Rev.*, 2014, **38**, 383–392, DOI: **10.1016/j.rser.2014.05.038**.

4 I. Ionel, I. A. Halmaciu, M. R. Wachter and S. Farsad, Bio-energy from municipal waste through anaerobic digestion or combustion?, *Eur. Biomass Conf. Exhib. Proc.*, 2022, 218–222, DOI: **10.5071/30thEUBCE2022-1CV.2.4**.

5 A. M. Omer, Green energies and the environment, *Renewable Sustainable Energy Rev.*, 2008, **12**, 1789–1821, DOI: **10.1016/J.RSER.2006.05.009**.

6 M. El ouardi, A. El Idrissi, M. Arab, M. Zbair, H. Haspel, M. Saadi and H. Ait Ahsaine, Review of photoelectrochemical water splitting: From quantitative approaches to effect of sacrificial agents, oxygen vacancies, thermal and magnetic field on (photo)electrolysis, *Int. J. Hydrogen Energy*, 2023, DOI: **10.1016/J.IJHYDENE.2023.09.111**.

7   W. Peng, F. Lü, L. Hao, H. Zhang, L. Shao and P. He, Digestate management for high-solid anaerobic digestion of organic wastes: A review, *Bioresour. Technol.*, 2020, **297**, 122485, DOI: 10.1016/j.biortech.2019.122485.

8   O. Golovko, L. Ahrens, J. Schelin, M. Sörengård, K. J. Bergstrand, H. Asp, M. Hultberg and K. Wiberg, Organic micropollutants, heavy metals and pathogens in anaerobic digestate based on food waste, *J. Environ. Manage.*, 2022, **313**, 114997, DOI: 10.1016/J.JENVMAN.2022.114997.

9   Z. Anfar, R. El Haouti, S. Lhanafi, M. Benafqir, Y. Azougarh and N. El Alem, Treated digested residue during anaerobic co-digestion of Agri-food organic waste: Methylene blue adsorption, mechanism and CCD-RSM design, *J. Environ. Chem. Eng.*, 2017, **5**, 5857–5867, DOI: 10.1016/j.jece.2017.11.015.

10 S.-H. Ho, Y. Chen, Z. Yang, D. Nagarajan, J.-S. Chang and N. Ren, High-efficiency removal of lead from wastewater by biochar derived from anaerobic digestion sludge, *Bioresour. Technol.*, 2017, **246**, 142–149, DOI: 10.1016/j.biortech.2017.08.025.

11 H. Ezz, M. G. Ibrahim, M. Fujii and M. Nasr, Enhanced Removal of Methylene Blue Dye by Sustainable Biochar Derived from Rice Straw Digestate, *Key Eng. Mater.*, 2022, **932**, 119–129, DOI: 10.4028/p-ss5269.

12 B. Jiang, Y. Lin and J. C. Mbog, Biochar derived from swine manure digestate and applied on the removals of heavy metals and antibiotics, *Bioresour. Technol.*, 2018, **270**, 603–611, DOI: 10.1016/j.biortech.2018.08.022.

13 J. Liu, S. Huang, K. Chen, T. Wang, M. Mei and J. Li, Preparation of biochar from food waste digestate: Pyrolysis behavior and product properties, *Bioresour. Technol.*, 2020, **302**, 122841, DOI: 10.1016/j.biortech.2020.122841.

14 Z. Anfar, M. Zbair, H. Ait Ahsiane, A. Jada and N. El Alem, Microwave assisted green synthesis of Fe_2O_3/biochar for ultrasonic removal of nonsteroidal anti-inflammatory pharmaceuticals, *RSC Adv.*, 2020, **10**, 11371–11380, DOI: 10.1039/D0RA00617C.

15 J. Zhao, Z. Wang, J. Li, B. Yan and G. Chen, Pyrolysis of food waste and food waste solid digestate: A comparative investigation, *Bioresour. Technol.*, 2022, **354**, 127191, DOI: 10.1016/j.biortech.2022.127191.

16 J. Liu, W. Zhang, M. Mei, T. Wang, S. Chen and J. Li, A Ca-rich biochar derived from food waste digestate with exceptional adsorption capacity for arsenic(III) removal via a cooperative mechanism, *Sep. Purif. Technol.*, 2022, **295**, 121359, DOI: 10.1016/j.seppur.2022.121359.

17 H. Chen, A. I. Osman, C. Mangwandi and D. Rooney, Upcycling food waste digestate for energy and heavy metal remediation applications, *Resour. Conserv. Recycl.: X.*, 2019, **3**, 100015, DOI: 10.1016/j.rcrx.2019.100015.

18 C. Zhang, S. Sun, S. Xu, C. Johnston and C. Wu, Phosphorus Removal from Dirty Farmyard Water by Activated Anaerobic-Digestion-Derived Biochar, *Ind. Eng. Chem. Res.*, 2022, DOI: 10.1021/acs.iecr.2c02668.

19 M. Gęca, M. Wiśniewska and P. Nowicki, Biochars and activated carbons as adsorbents of inorganic and organic compounds from multicomponent systems – A review, *Adv. Colloid Interface Sci.*, 2022, **305**, 102687, DOI: 10.1016/j.cis.2022.102687.

20 A. Ait El Fakir, Z. Anfar, M. Enneiymy, A. Jada and N. El Alem, New insights into N, S doped carbon from conjugated polymers for efficient persulfate activation: Role of hydrogel beads in enhancement of stability, *Chem. Eng. J.*, 2022, **442**, 136055, DOI: 10.1016/J.CEJ.2022.136055.

21 B. E. Channab, M. El Ouardi, S. E. Marrane, O. A. Layachi, A. El Idrissi, S. Farsad, D. Mazkad, A. BaQais, M. Lasri and H. Ait Ahsaine, Alginate@$ZnCO_2O_4$ for efficient peroxymonosulfate activation towards effective rhodamine B degradation: optimization using response surface methodology, *RSC Adv.*, 2023, **13**, 20150–20163, DOI: 10.1039/D3RA02865H.

22 A. El Idrissi, O. Dardari, F. N. N. N. Metomo, Y. Essamlali, A. Akil, O. Amadine, S. Aboulhrouz and M. Zahouily, Effect of sodium alginate-based superabsorbent hydrogel on tomato growth under different water deficit conditions, *Int. J. Biol. Macromol.*, 2023, **253**, 127229, DOI: 10.1016/J.IJBIOMAC.2023.127229.

23 A. Ait El Fakir, Z. Anfar, A. Amedlous, M. Zbair, Z. Hafidi, M. El Achouri, A. Jada and N. El Alem, Engineering of new hydrogel beads based conducting polymers: Metal-free catalysis for highly organic pollutants degradation, *Appl. Catal., B*, 2021, **286**, 119948, DOI: 10.1016/j.apcatb.2021.119948.

24 Z. Anfar, A. Amedlous, A. A. El Fakir, M. Zbair, H. Ait Ahsaine, A. Jada and N. El Alem, High extent mass recovery of alginate hydrogel beads network based on immobilized bio-sourced porous carbon@Fe_3O_4-NPs for organic pollutants uptake, *Chemosphere*, 2019, **236**, 124351, DOI: 10.1016/j.chemosphere.2019.124351.

25 K. Aziz, M. El Achaby, R. Mamouni, N. Saffaj and F. Aziz, A novel hydrogel beads based copper-doped Cerastoderma edule shells@Alginate biocomposite for highly fungicide sorption from aqueous medium, *Chemosphere*, 2023, **311**, 136932, DOI: 10.1016/j.chemosphere.2022.136932.

26 M. Salimi, B. Channab, A. El Idrissi, M. Zahouily and E. Motamedi, A comprehensive review on starch: Structure, modification, and applications in slow/controlled-release fertilizers in agriculture, *Carbohydr. Polym.*, 2023, **322**, 121326, DOI: 10.1016/j.carbpol.2023.121326.

27 L. Gao, Z. Li, W. Yi, L. Wang, N. Song, W. Zhang, G. Li, S. Wang, N. Li and A. Zhang, Effective Pb^{2+} adsorption by calcium alginate/modified cotton stalk biochar aerogel spheres: With application in actual wastewater, *J. Environ. Chem. Eng.*, 2023, **11**, 109074, DOI: 10.1016/j.jece.2022.109074.

28 J. Chen, J. Ouyang, X. Cai, X. Xing, L. Zhou, Z. Liu and D. Cai, Removal of ciprofloxacin from water by millimeter-sized sodium alginate/H_3PO_4 activated corncob-based biochar composite beads, *Sep. Purif. Technol.*, 2021, **276**, 119371, DOI: 10.1016/j.seppur.2021.119371.

29 B. Deepanraj, V. Sivasubramanian and S. Jayaraj, Experimental and kinetic study on anaerobic digestion of food waste: The effect of total solids and pH, *J. Renewable Sustainable Energy*, 2015, **7**, 063104, DOI: 10.1063/1.4935559.

30 F. Lü, X. Xu, L. Shao and P. He, Importance of storage time in mesophilic anaerobic digestion of food waste, *J. Environ. Sci.*, 2016, **45**, 76–83, DOI: 10.1016/J.JES.2015.11.019.

31 S. Farsad, Z. Anfar, A. Ait El Fakir, A. Amjlef, N. El Alem and I. Ionel, Methane recovery from the leachate of municipal solid waste landfill by using anaerobic digestion. Case study, *Eur. Biomass Conf. Exhib. Proc.*, 2022, 223–227, DOI: **10.5071/30thEUBCE2022-1CV.2.5**.

32 S. Fan, J. Tang, Y. Wang, H. Li, H. Zhang, J. Tang, Z. Wang and X. Li, Biochar prepared from co-pyrolysis of municipal sewage sludge and tea waste for the adsorption of methylene blue from aqueous solutions: Kinetics, isotherm, thermodynamic and mechanism, *J. Mol. Liq.*, 2016, **220**, 432–441, DOI: **10.1016/J.MOLLIQ.2016.04.107**.

33 S. Fan, Y. Wang, Z. Wang, J. Tang, J. Tang and X. Li, Removal of methylene blue from aqueous solution by sewage sludge-derived biochar: Adsorption kinetics, equilibrium, thermodynamics and mechanism, *J. Environ. Chem. Eng.*, 2017, **5**, 601–611, DOI: **10.1016/J.JECE.2016.12.019**.

34 T. Manoharan, S. Ganeshalingam and K. Nadarajah, Mechanisms of emerging contaminants removal by novel neem chip biochar, *Environ. Adv.*, 2022, **7**, 100158, DOI: **10.1016/J.ENVADV.2021.100158**.

35 Z. Anfar, R. El Haouti, S. Lhanafi, M. Benafqir, Y. Azougarh and N. El Alem, Treated digested residue during anaerobic co-digestion of Agri-food organic waste: Methylene blue adsorption, mechanism and CCD-RSM design, *J. Environ. Chem. Eng.*, 2017, **5**, 5857–5867, DOI: **10.1016/J.JECE.2017.11.015**.

36 B. Ji, J. Wang, H. Song and W. Chen, Removal of methylene blue from aqueous solutions using biochar derived from a fallen leaf by slow pyrolysis: Behavior and mechanism, *J. Environ. Chem. Eng.*, 2019, **7**, 103036, DOI: **10.1016/J.JECE.2019.103036**.

37 H. Ait Ahsaine, M. Zbair, Z. Anfar, Y. Naciri, R. El haouti, N. El Alem and M. Ezahri, Cationic dyes adsorption onto high surface area 'almond shell' activated carbon: Kinetics, equilibrium isotherms and surface statistical modeling, *Mater. Today Chem.*, 2018, **8**, 121–132, DOI: **10.1016/J.MTCHEM.2018.03.004**.

38 M. Zbair, H. Ait Ahsaine, Z. Anfar and A. Slassi, Carbon microspheres derived from walnut shell: Rapid and remarkable uptake of heavy metal ions, molecular computational study and surface modeling, *Chemosphere*, 2019, **231**, 140–150, DOI: **10.1016/J.CHEMOSPHERE.2019.05.120**.

39 H. Panda, N. Tiadi, M. Mohanty and C. R. Mohanty, Studies on adsorption behavior of an industrial waste for removal of chromium from aqueous solution, *S. Afr. J. Chem. Eng.*, 2017, **23**, 132–138, DOI: **10.1016/J.SAJCE.2017.05.002**.

40 Z. Anfar, M. Zbair, H. A. Ahsaine, Y. Abdellaoui, A. A. El Fakir, E. H. Amaterz, A. Jada and N. El Alem, Preparation and Characterization of Porous Carbon@ZnO-NPs for Organic Compounds Removal: Classical Adsorption Versus Ultrasound Assisted Adsorption, *ChemistrySelect*, 2019, **4**, 4981–4994, DOI: **10.1002/SLCT.201901043**.

41 M. Benafqir, Z. Anfar, M. Abbaz, R. El Haouti, S. Lhanafi, Y. Azougarh, A. Ait El Fakir, M. Ez-zahery and N. El Alem, Hematite–titaniferous sand as a new low-cost adsorbent for orthophosphates removal: Adsorption, mechanism and Process Capability study, *Environ. Technol. Innovation*, 2019, **13**, 153–165, DOI: **10.1016/J.ETI.2018.10.009**.

42 A. Amjlef, S. Khrach, A. Ait El Fakir, S. Farsad, S. Et-Taleb and N. El Alem, Adsorptive properties investigation of natural sand as adsorbent for methylene blue removal from contaminated water, *Nanotechnol. Environ. Eng.*, 2021, **6**, 1–15, DOI: **10.1007/S41204-021-00119-Y/FIGURES/14**.

43 N. Ouasfi, M. Zbair, E. M. Sabbar and L. Khamliche, High performance of Zn–Al–CO3 layered double hydroxide for anionic reactive blue 21 dye adsorption: kinetic, equilibrium, and thermodynamic studies, *Nanotechnol. Environ. Eng.*, 2019, **4**, 1–13, DOI: **10.1007/S41204-019-0063-5/TABLES/7**.

44 A. Amjlef, S. Farsad, A. Ait El Fakir, A. El Asri, S. El Issami, S. Et-Taleb and N. El Alem, Polyaniline-encapsulated quartz sand as an adsorbent composite for Orange G dye removal from aqueous solution: Experimental and computational study, *Ceram. Int.*, 2023, **49**, 14120–14134, DOI: **10.1016/J.CERAMINT.2022.12.293**.

45 M. Gao, D. Xu, Y. Gao, G. Chen, R. Zhai, X. Huang, X. Xu, J. Wang, X. Yang and G. Liu, Mussel-inspired triple bionic adsorbent: Facile preparation of layered double hydroxide@polydopamine@metal-polyphenol networks and their selective adsorption of dyes in single and binary systems, *J. Hazard. Mater.*, 2021, **420**, 126609, DOI: **10.1016/J.JHAZMAT.2021.126609**.

46 X. Zhao, X. Wang and T. Lou, Preparation of fibrous chitosan/sodium alginate composite foams for the adsorption of cationic and anionic dyes, *J. Hazard. Mater.*, 2021, **403**, 124054, DOI: **10.1016/J.JHAZMAT.2020.124054**.

47 H. Ezz, M. G. Ibrahim, M. Fujii and M. Nasr, Enhanced Removal of Methylene Blue Dye by Sustainable Biochar Derived from Rice Straw Digestate, *Key Eng. Mater.*, 2022, **932**, 119–129, DOI: **10.4028/P-SS5269**.

48 S. Sahu, S. Pahi, S. Tripathy, S. K. Singh, A. Behera, U. K. Sahu and R. K. Patel, Adsorption of methylene blue on chemically modified lychee seed biochar: Dynamic, equilibrium, and thermodynamic study, *J. Mol. Liq.*, 2020, **315**, 113743, DOI: **10.1016/J.MOLLIQ.2020.113743**.

49 M. A. Islam, M. J. Ahmed, W. A. Khanday, M. Asif and B. H. Hameed, Mesoporous activated coconut shell-derived hydrochar prepared via hydrothermal carbonization-NaOH activation for methylene blue adsorption, *J. Environ. Manage.*, 2017, **203**, 237–244, DOI: **10.1016/J.JENVMAN.2017.07.029**.

50 S. Fan, Y. Wang, Z. Wang, J. Tang, J. Tang and X. Li, Removal of methylene blue from aqueous solution by sewage sludge-derived biochar: Adsorption kinetics, equilibrium, thermodynamics and mechanism, *J. Environ. Chem. Eng.*, 2017, **5**, 601–611, DOI: **10.1016/J.JECE.2016.12.019**.

51 Y. M. Wu, J. Yang, X. L. Fan, S. F. Fu, M. T. Sun and R. B. Guo, Elimination of methane in exhaust gas from biogas upgrading process by immobilized methane-oxidizing bacteria, *Bioresour. Technol.*, 2017, **231**, 124–128, DOI: **10.1016/J.BIORTECH.2017.01.020**.

52 B. Ji, J. Wang, H. Song and W. Chen, Removal of methylene blue from aqueous solutions using biochar derived from a fallen leaf

by slow pyrolysis: Behavior and mechanism, *J. Environ. Chem. Eng.*, 2019, **7**, 103036, DOI: **10.1016/J.JECE.2019.103036**.

53 S. Fan, Y. Wang, Z. Wang, J. Tang, J. Tang and X. Li, Removal of methylene blue from aqueous solution by sewage sludge-derived biochar: Adsorption kinetics, equilibrium, thermo-dynamics and mechanism, *J. Environ. Chem. Eng.*, 2017, **5**, 601–611, DOI: **10.1016/J.JECE.2016.12.019**.

54 L. Liu, Y. Li and S. Fan, Preparation of KOH and H3PO4 Modified Biochar and Its Application in Methylene Blue Removal from Aqueous Solution, *Processes*, 2019, **7**, 891, DOI: **10.3390/PR7120891**.

55 C. Yang, H. Wu, M. Cai, Y. Li, C. Guo, Y. Han, Y. Zhang and B. Song, Valorization of food waste digestate to ash and biochar composites for high performance adsorption of methylene blue, *J. Cleaner Prod.*, 2023, **397**, 136612, DOI: **10.1016/J.JCLEPRO.2023.136612**.

56 Z. Anfar, A. Amedlous, A. Ait El Fakir, H. Ait Ahsaine, M. Zbair, S. Lhanafi, R. El Haouti, A. Jada and N. El Alem, Combined Methane Energy Recovery and Toxic Dye Removal by Porous Carbon Derived from Anaerobically Modified Digestate, *ACS Omega*, 2019, **4**, 9434–9445, DOI: **10.1021/acsomega.9b00524**.